Dovepress

ORIGINAL RESEARCH

Clinical Application of a Graphene Oxide-Based Surface Plasmon Resonance Biosensor to Measure First-Trimester Serum Pregnancy-Associated Plasma Protein-A/A2 Ratio to Predict Preeclampsia

Chen-Yu Chen [1,2], Ying-Hao Wang[1], Chie-Pein Chen[1], Fang-Ju Sun[3], Yi-Yung Chen[1], Yu-Jun Huang[1], Nan-Fu Chiu [4,5]

[1]Department of Obstetrics and Gynecology, MacKay Memorial Hospital, Taipei, 10449, Taiwan; [2]Department of Medicine, MacKay Medical College, New Taipei City, 252005, Taiwan; [3]Department of Medical Research, MacKay Memorial Hospital, Taipei, 10449, Taiwan; [4]Laboratory of Nano-Photonics and Biosensors, Institute of Electro-Optical Engineering, National Taiwan Normal University, Taipei, 11677, Taiwan; [5]Department of Life Science, National Taiwan Normal University, Taipei, 11677, Taiwan

Correspondence: Chen-Yu Chen, Department of Obstetrics and Gynecology, MacKay Memorial Hospital, No. 92, Section 2, Zhong-Shan North Road, Taipei, 10449, Taiwan, Tel +886-2-25433535, Fax +886-2-25433642, Email f122481@mmh.org.tw; Nan-Fu Chiu, Laboratory of Nano-Photonics and Biosensors, Institute of Electro-Optical Engineering, National Taiwan Normal University, No. 88, Section 4, Ting-Chou Road, Taipei, 11677, Taiwan, Tel +886-2-77496722, Fax +886-2-86631954, Email nfchiu@ntnu.edu.tw

Background: Preeclampsia, a major cause of adverse pregnancy outcomes, involves metalloproteinases pregnancy-associated plasma protein (PAPP)-A and PAPP-A2 from placental trophoblasts. The graphene oxide (GO)-based surface plasmon resonance (SPR) biosensor has higher sensitivity, affinity, and selective ability than the traditional SPR biosensor. The aim of this study was to explore the feasibility of measuring first-trimester serum PAPP-A/PAPP-A2 ratio as a novel predictor of preeclampsia using the GO-SPR biosensor.

Methods: This prospective case-control study of pregnant women was conducted at MacKay Memorial Hospital, Taipei, Taiwan between January 2018 and June 2020. The SPR angle shifts of first-trimester serum PAPP-A, PAPP-A2, and PAPP-A/PAPP-A2 ratio measured using the GO-SPR biosensor were compared between preeclampsia and control groups.

Results: Serum samples from 185 pregnant women were collected, of whom 30 had preeclampsia (5 early-onset; 25 late-onset). The response time between the antibody-antigen association and dissociation only took about 200 seconds. The SPR angle shift of PAPP-A in the preeclampsia group was significantly smaller than that in the control group (median (interquartile range): 5.33 (4.55) versus 6.89 (4.10) millidegrees (mDeg), $P = 0.008$). Conversely, the SPR angle shift of PAPP-A2 in the preeclampsia group was significantly larger than that in the control group (5.70 (3.81) versus 3.63 (2.38) mDeg, $P < 0.001$). Receiver operating characteristic (ROC) curve analysis revealed a cut-off PAPP-A/PAPP-A2 ratio to predict all preeclampsia of ≤ 0.76, with an area under the ROC curve (AUC) of 0.79 (95% CI 0.73–0.85, $P < 0.001$). Sub-group analysis revealed a cut-off PAPP-A/PAPP-A2 ratio to predict early-onset preeclampsia of ≤ 0.53 (AUC 0.99, 95% CI 0.96–1.00, $P < 0.001$), and ≤ 0.73 to predict late-onset preeclampsia (AUC 0.75, 95% CI 0.68–0.81, $P < 0.001$).

Conclusion: Measuring first-trimester serum PAPP-A/PAPP-A2 ratio using the GO-SPR biosensor could be a valuable method for early prediction of preeclampsia.

Keywords: graphene oxide, surface plasmon resonance, biosensor, preeclampsia, PAPP-A/PAPP-A2 ratio

Introduction

Preeclampsia is a life-threatening disorder which affects 2–8% of pregnancies, and it is one of the major causes of adverse pregnancy outcomes.[1] Preeclampsia is classified as being early-onset (< 34 gestational weeks) or late-onset (≥ 34 gestational weeks), of which early-onset preeclampsia is less prevalent but has worse outcomes than late-onset preeclampsia.[2] The pathophysiology of preeclampsia remains uncertain, however it is well-recognized that an ischemic

Graphical Abstract
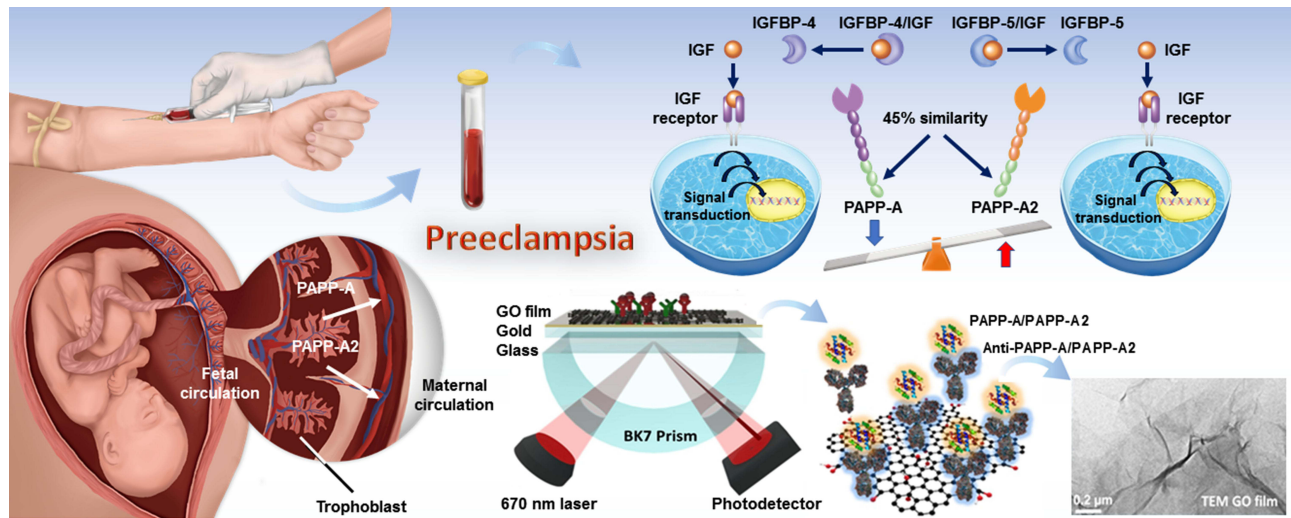
placenta plays a critical role because it releases various biochemical factors into the maternal circulation, which change maternal systemic endothelial function resulted in hypertension and other features of preeclampsia.[3]

The insulin-like growth factor (IGF) system is thought to play a crucial role in the pathogenesis of preeclampsia.[4] Quantification of maternal serum proteins related to the IGF family can be used in preeclampsia screening. Pregnancy-associated plasma protein A (PAPP-A), a 200 kDa metzincin superfamily metalloproteinase, originates primarily from placental trophoblasts. PAPP-A is an imperative protease that can cleave insulin-like growth factor binding protein (IGFBP)-4 to release IGFs, which bind IGF receptors and activate the IGF pathway to facilitate trophoblast invasion and vascular remodeling.[5] Pregnancy-associated plasma protein A2 (PAPP-A2), a novel 220 kDa metalloproteinase, is also mostly produced by placental trophoblasts and specifically cleaves IGFBP-5 to release IGFs.[6] PAPP-A2 is a homologue of PAPP-A, and they share 45% amino acid residues.[6] Although both PAPP-A and PAPP-A2 affect placentation and fetal growth via the regulation of IGF bioavailability, they have dissimilar physiological functions and can be potential biomarkers to predict preeclampsia.[7–10] Low PAPP-A levels result in diminished IGF signaling, indicating impaired trophoblast invasion and placental perfusion, leading to placental hypoxia and oxidative stress in preeclampsia. Conversely, elevated PAPP-A2 levels may contribute to abnormal placentation, reducing blood flow, inducing hypoxia, and fostering endothelial dysfunction in preeclampsia. These imbalances underscore the vascular and placental abnormalities characteristic of this condition. Previous studies have demonstrated that a lower level of first-trimester PAPP-A is associated with an increased risk of preeclampsia,[7,8] while a higher level of PAPP-A2 is associated with an increased risk of preeclampsia.[9,10]

Various biosensors for early detection of biomarkers related to preeclampsia have become available in recent years.[11–17] Two-dimensional graphene materials have been proven to have excellent biocompatibility in biomedical applications such as biomarker detection, antibacterial surfaces, and drug carriers.[18–20] Graphene oxide (GO), a derivative compound of graphene, is chemically modified graphene that contains many functional epoxy, hydroxyl, carbonyl, and carboxyl groups, which result in excellent amphiphilicity.[21–23] In addition, GO has semiconductor characteristics, and when combined with gold (Au) films it can form a perfect heterostructure interface, which can enhance the surface plasmon resonance (SPR) response.[24,25] Therefore, it has become an increasingly important nanomaterial for assay applications in biomedical optoelectronics.[25–28]

In clinical practice, the only definite therapy for preeclampsia is termination of pregnancy and complete removal of the placenta, however preterm birth and perinatal death can also occur. Predicting the women at risk of preeclampsia as early as possible allows for prophylactic procedures such as the early use of low-dose aspirin to decrease the development of preeclampsia.[29,30] PAPP-A has been widely used in first-trimester preeclampsia screening;[30,31] however, PAPP-A2 was

discovered after PAPP-A and it has not been used in clinical practice. In this study, we tried to use a GO-SPR biosensor to examine the SPR angle shifts of serum PAPP-A and PAPP-A2 of first-trimester pregnant women to predict preeclampsia. In addition, we compared the SPR angle shifts of PAPP-A, PAPP-A2, and PAPP-A/PAPP-A2 ratio, and further investigated the feasibility of using PAPP-A/PAPP-A2 ratio as a novel index of preeclampsia.

Materials and Methods

Sample Collection

We conducted this prospective case-control study at a tertiary referral hospital in Taipei, Taiwan between January 2018 and June 2020. Serum samples were collected from pregnant women who underwent aneuploidy screening in the first trimester of pregnancy (11 0/7 to 13 6/7 gestational weeks). The exclusion criteria were: women with underlying chronic diseases, fetal structural or chromosomal anomalies, and multifetal pregnancies. Preeclampsia was diagnosed as hypertension (systolic blood pressure ≥ 140 mm-Hg and/or diastolic blood pressure ≥ 90 mm-Hg) detected after 20 gestational weeks with proteinuria or end-organ dysfunction.[32] Preeclampsia was classified as either early-onset (< 34 gestational weeks) or late-onset (≥ 34 gestational weeks), and it resolved only after delivery. Therefore, a case of early-onset preeclampsia would not simultaneously be a case of late-onset preeclampsia. This study was performed following the ethical policies and procedures approved by the Institutional Review Board of MacKay Memorial Hospital (Approval no. 16MMHIS149). Informed consent was obtained from the participants, and the personal identifiers were anonymized before analysis. All methods were performed in accordance with the ethical standards of the Declaration of Helsinki.

Maternal blood samples, approximately 3 mL in volume, were collected for aneuploidy screening. Upon centrifugation, the serum was separated and stored at −20°C until analysis. PAPP-A concentrations were measured by time-resolved amplified cryptate emission (TRACE) technology (Thermo Fisher Scientific). The PAPP-A in the serum samples was sandwiched between two diverse monoclonal antibodies, the first conjugated with europium cryptate, and the other with the fluorophore, allophycocyanin (APC, XL665). The basis of TRACE technology is non-radiative fluorescence energy transfer from a donor (europium cryptate) to an acceptor (XL 665) measured using a KRYPTOR analyzer (Thermo Fisher Scientific). In addition, PAPP-A2 concentrations were measured by a commercial enzyme-linked immunosorbent assay (ELISA) (MBS012098, MyBioSource). The assay was conducted according to the manu-facturer's protocol, and the absorbance was measured at 450 nm. The samples were then taken to our laboratory to examine the SPR angle shifts of PAPP-A and PAPP-A2 using the GO-based SPR biosensor.

Preparation of the GO-Based SPR Nanochip

Figure 1A shows the real picture of a GO-based SPR chip. Figure 1B shows the GO-based SPR biosensor system with its biomolecule binding and sensing mechanism. GO sheets were exfoliated from natural graphene by the modified Hummers' method. The biosensor, featuring a tailored ligand coating for specific interaction with PAPP-A and PAPP-A2 proteins, was situated over a BK7 prism. A laser emitting at a precise wavelength of 670 nm was directed onto the biosensor to initiate the SPR phenomenon. The BK7 prism facilitated the transmission of laser light through the biosensor, enabling interaction with the blood samples. Interactions between PAPP-A and PAPP-A2 in the samples and the immobilized ligands induced changes in the SPR angle. This alteration was meticulously monitored in real-time by a highly sensitive photodetector. Immunoassay reactions were performed by a sensing film of GO sheets concentration of 1 mg/mL at a film thickness of about 1.8 nm by adsorbed to the Au film (47 nm) surface.[33] After the GO sheets had been adsorbed, the surface thickness of the Au film coated with the linker cystamine dihydrochloride (Cys, 98%, Alfa Aesar).[34] Cystamine contains amine and thiol functional groups, and we used cystamine to generate thiol self-assembled monolayers (SAMs) on the bare Au film surfaces. The carboxyl-GO sheet was immobilized on the Au film as a carboxyl-GO sensing layer. This carboxyl-GO sensing layer and cystamine formed a covalent bond by chemical reactions with -COOH and -NH2.[35] The dispersion and surface morphology of the GO sheets were analyzed using a transmission electron microscope (TEM) (FEI Tecnai G20, Hillsboro, OR, USA). Figure 1C shows the interactions between GO functional groups and protein molecules. The surface of the GO sheets was rich in oxidizing functional groups (epoxy, hydroxyl, carbonyl, and carboxyl), which enhanced the bio-affinity. The carboxyl groups of the GO sheets
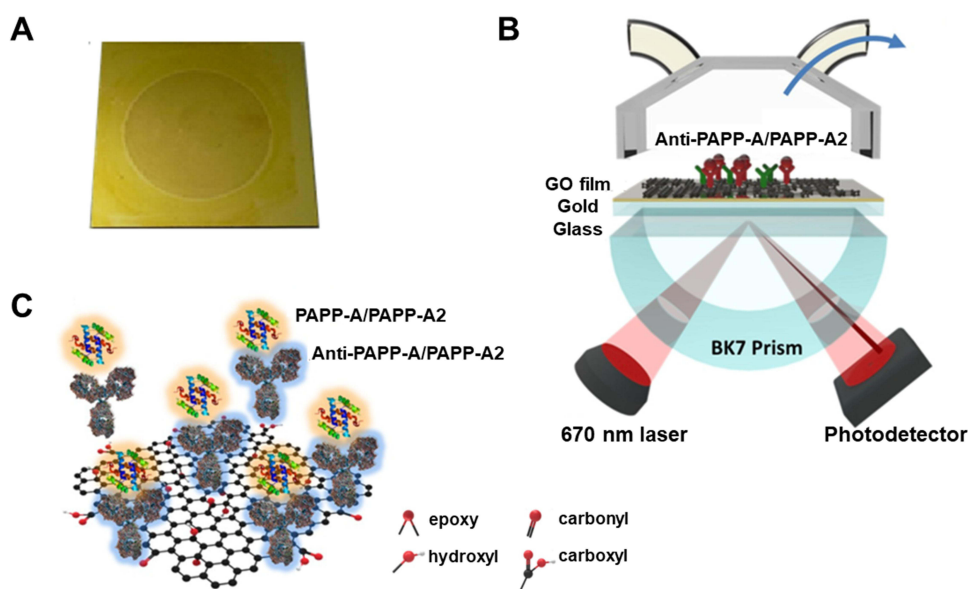
Figure 1 The sensing mechanism of the GO-SPR biosensor to measure PAPP-A and PAPP-A2. (**A**) The real picture of a GO-based SPR chip. (**B**) A schematic diagram of the GO-SPR biosensor. The 1 mg/mL GO sheet (1.8 nm) is immobilized on the Au film (47 nm) surface. (**C**) The interactions between GO functional groups and protein molecules. The surface of the GO sheets is rich in oxidizing functional groups which enhance the bio-affinity.

could form a chemical covalent bond with the amino groups of antibodies (anti-PAPP-A (MBS668449, MyBioSource) and anti-PAPP-A2 (MBS690059, MyBioSource)). This GO-protein covalent bond can be utilized by SPR technology for immunoassay biochips.
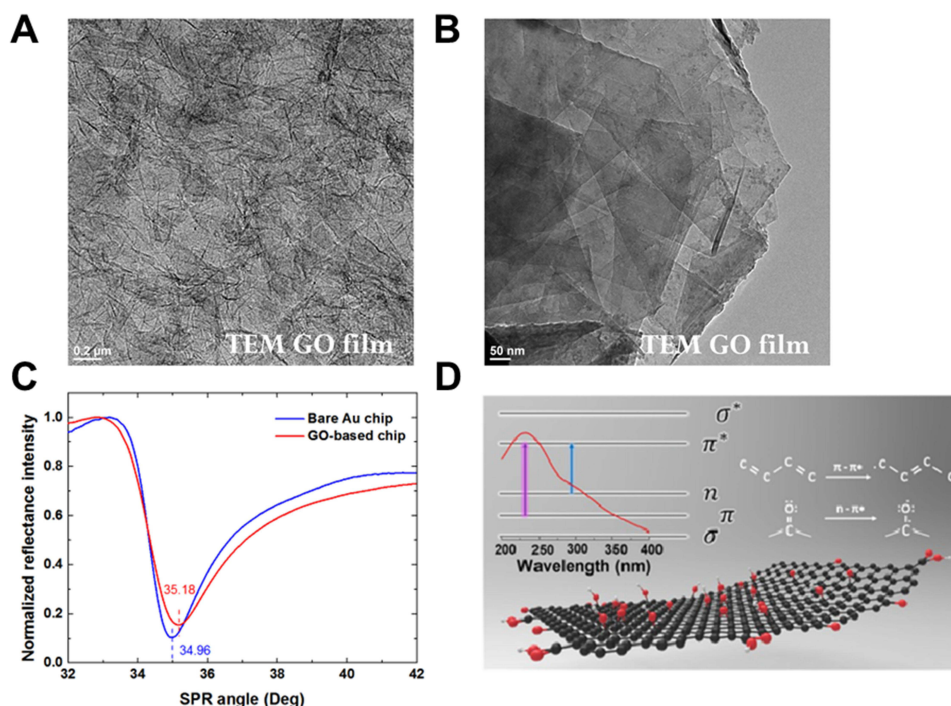
Microscopic Morphology and Chemical Structure of GO Sheets

The TEM images in Figure 2A and B display different amplifications of a GO sheet with a layer-by-layer lamination and organic shell matrix structure, where 0.275 mg/mL GO immobilized on the surface of the Au film. In Figure 2B, the TEM image features a 50 nm ruler scale, and the observed stacked and wrinkled flakes suggest that most GO sheets have a diameter of less than 50 nm. Figure 2C shows the resonance angular shifts of bare Au chips and GO-based chips under the incident light of 690 nm using the Kretschmann configuration system. The SPR angular displacements of bare Au and GO-based chips were 34.96° and 35.18°, respectively. The results showed that the thin film layer of the GO-based chip leaded to a larger SPR angle, which verified that the GO sheets were modified on the surface of Au film. Figure 2D shows the ultraviolet-visible (UV-Vis) absorption spectrum and chemical structure of the GO sheets. The UV-Vis absorption spectrum of oxygen-containing carbon groups in aqueous GO dispersion yielded two absorption peaks: an absorption peak at around 230 nm, which represented the π–π* absorption peak of aromatic C-C bonds in different aromatic sp2 cluster sizes, and a weak shoulder at around 300 nm, which represented the n–π* absorption peak because of epoxy and carbonyl bonds.

Optimization of Antibody Immobilization and Pre-Analytic Sample Processing

Figure S1 shows real-time SPR sensorgrams of response curves for the assay of anti-PAPP-A anti-PAPP-A2 immobilization processing steps. Initially, the carboxyl groups of the GO sheets were activated by 0.4 M 1-ethyl-3-(3-dimethyla-minopropyl) carbodiimide (EDC, Sigma-Aldrich) and 0.1 M N-hydroxysuccinimide (NHS, Sigma-Aldrich), with a flow rate of 60 μL/min and an injection volume of 200 μL. We then immobilized 25 μg/mL anti-PAPP-A or 25 μg/mL anti-PAPP-A2 on the surface of the chip at a flow rate of 10 μL/min, and used 1 mg/mL bovine serum albumin (BSA, pH 7, ≥ 98%, Sigma-Aldrich) to reduce non-specific binding proteins on the chip surface. After that we injected 1 M ethanolamine hydrochloride (EA, Sigma-Aldrich) to stop the remaining activation of the functional groups. In the last step, we injected 10 mM of sodium hydroxide (NaOH, Sigma-Aldrich, USA) at a flow rate of 60 μL/min.

Figure 2 Microscopic morphology and chemical structure of GO sheets. (**A** and **B**) High-resolution TEM images of a GO sheet with a layer-by-layer lamination and organic shell matrix structure. In Figure 2B, the TEM image features a 50 nm ruler scale, and the observed stacked and wrinkled flakes suggest that most GO sheets have a diameter of less than 50 nm. (**C**) The graph of SPR characteristic curves between bare Au chips and GO-based chips, which was generated using the OriginPro 9.1 software. The SPR angular displacements of bare Au and GO-based chips are 34.96° and 35.18°, respectively. (**D**) The UV-Vis absorption spectrum and chemical structure of GO sheets. An absorption peak at around 230 nm represents the π–π* absorption peak of aromatic C-C bonds in different aromatic sp2 cluster sizes, and a weak shoulder at around 300 nm represents the n–π* absorption peak because of epoxy and carbonyl bonds.

The serum samples were diluted 100, 1000 and 10,000 times with running buffer at different pH levels to detect PAPP-A and PAPP-A2 using the GO-SPR biosensor (Figure S2). The running buffer contained 1 mg/mL BSA, 200 mM NaCl, 0.05% Tween-20 (1 g/mL, Sigma-Aldrich), and 1x (100 mL) phosphate buffer saline (PBS, UniRegion Bio-Tech). The isoelectric point of IgG antibody ranged between 6.8 and 8.5. Running buffers with different pH values were compared to reduce non-specific binding. A BI-3000 SPR system (Biosensing Instrument) was used to examine the SPR angle shifts of PAPP-A and PAPP-A2 in clinical samples, and 50 mM of NaOH was used to regenerate the chip surface. The response time between the antibody-antigen association and dissociation only took about 200 seconds. The SPR angle shifts of serum samples, diluted 1000-fold, closely approximated those of the standard antigens.[17] In this experiment, each sample was diluted 1000 times with running buffer in a volume of 250 μL and injected at a flow rate of 60 μL/min at pH 7.4 and room temperature for measuring PAPP-A and PAPP-A2.

Data Analysis

We used SPSS version 24.0 (IBM Corporation, Armonk, USA) and SAS version 9.4 (SAS Institute, Cary, USA) for statistical analyses. Spearman correlation analysis was used to evaluate correlations between SPR angle shifts and values of commercial assays. The Kolmogorov–Smirnov test was conducted to evaluate whether the continuous variables showed a normal distribution. Upon recognizing that the data did not adhere to a normal distribution, we subsequently employed the Mann–Whitney *U*-test and presented the data using the median (interquartile range). Receiver Operating Characteristic (ROC) curves, along with the Youden Index, were employed to determine the cut-off values for PAPP-A, PAPP-A2, and PAPP-A/PAPP-A2 ratio in predicting preeclampsia. The threshold for determining the detection rate was set at 0.5. The confusion matrix was employed to validate the predictive performance of PAPP-A, PAPP-A2, and PAPP-A/PAPP-A2 ratio. We utilized a paired sample design to assess ROC contrast estimates, accounting for the correlation between tests on the same subjects in predicting preeclampsia. A *P* value < 0.05 was considered to be statistically significant.

Results

Calibration Curves Between the Results of the GO-SPR Biosensor and Commercial Assays

The initial 45 serum samples from pregnant women were used to establish calibration curves correlating SPR angle shifts with values from commercial biochemical assays (PAPP-A measured by TRACE technology and PAPP-A2 measured by ELISA). Strong correlations were observed for measuring PAPP-A ($r = 0.966$) and PAPP-A2 ($r = 0.957$) between the experimental values obtained using the GO-SPR biosensor and commercial methods (Figure 3A and B).

SPR Angle Shifts of PAPP-A and PAPP-A2 in Clinical Samples

We totally collected 185 serum samples from the pregnant women, of them 30 were diagnosed with preeclampsia (5 early-onset and 25 late-onset). Table 1 presents maternal characteristics, laboratory data, and neonatal outcomes. The SPR angle shift of PAPP-A in the preeclampsia group was significantly smaller than that in the control group (5.33 (4.55) versus 6.89 (4.10) mDeg, $P = 0.008$). Furthermore, the SPR angle shift of PAPP-A2 in the preeclampsia group was significantly larger than that in the control group (5.70 (3.81) versus 3.63 (2.38) mDeg, $P < 0.001$) (Figure 3C). The converted concentrations of PAPP-A and PAPP-A2, calculated from the SPR angle shift results, were 2.27 (2.16) versus 3.01 (1.94) (IU/L) and 5.07 (4.82) versus 2.45 (3.01) (ng/mL) in the preeclampsia group and the control group, respectively. Sub-group analysis revealed that there was no significant difference in PAPP-A SPR angle shift between early-onset (4.28 ± 1.79 mDeg) and late-onset (6.51 ± 3.92 mDeg) preeclampsia ($P = 0.229$), but that PAPP-A2 SPR
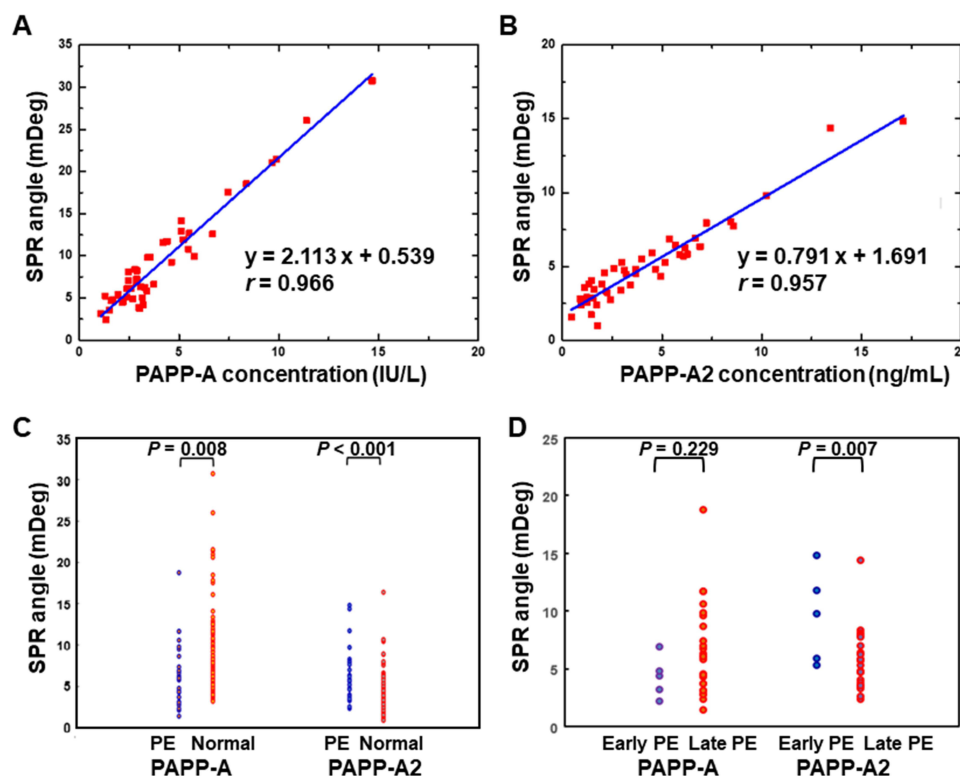
Figure 3 SPR angle shifts of PAPP-A and PAPP-A2 in clinical samples. (**A** and **B**) Relationships between SPR angle shifts and values of commercial assays for measuring PAPP-A ($r = 0.966$) and PAPP-A2 ($r = 0.957$). (**C**) SPR angle shifts of PAPP-A and PAPP-A2 in the preeclampsia and normal groups. The SPR angle shift of PAPP-A in the preeclampsia group 5.33 (4.55 mDeg) is significantly smaller than that in the control group 6.89 (4.10 mDeg) ($P = 0.008$). The SPR angle shift of PAPP-A2 in the preeclampsia group 5.70 (3.81 mDeg) is significantly larger than that in the control group 3.63 (2.38 mDeg) ($P < 0.001$). (**D**) SPR angle shifts of PAPP-A and PAPP-A2 in the early- and late-onset preeclampsia groups. PAPP-A2 SPR angle shift in the early-onset preeclampsia group (9.53 ± 16.16 mDeg) is significantly larger than that in the late-onset preeclampsia group (5.60 ± 6.27 mDeg) ($P = 0.007$).
Abbreviation: PE, preeclampsia.

Table 1 Maternal Characteristics, Laboratory Data, and Neonatal Outcomes

	Preeclampsia (n = 30)	No Preeclampsia (n = 155)	P value
Mother			
Age (year)	34.0 (7.0)	32.0 (5.0)	0.023*
Weight (kg)	58.0 (20.5)	53.4 (11.0)	0.047*
Gravida	1.0 (1.0)	2.0 (1.0)	0.546
Para	1.0 (1.0)	1.0 (1.0)	0.171
Delivery age (week)	38.3 (2.3)	39.3 (1.7)	0.001*
Chronic hypertension	6 (20.0%)	3 (1.9%)	0.001*
Diabetes mellitus	2 (6.7%)	5 (3.2%)	0.317
Cesarean delivery	8 (26.7%)	32 (20.8%)	0.474
First-trimester examination			
Detection time (week)	13.0 (0.5)	12.7 (0.6)	0.055
PAPP-A (mDeg)	5.33 (4.55)	6.89 (4.10)	0.008*
Converted PAPP-A (IU/L)	2.27 (2.16)	3.01 (1.94)	0.008*
PAPP-A2 (mDeg)	5.70 (3.81)	3.63 (2.38)	< 0.001*
Converted PAPP-A2 (ng/mL)	5.07 (4.82)	2.45 (3.01)	< 0.001*
Neonate			
Birth age (week)	38.3 (2.3)	39.3 (1.7)	0.001*
Birth weight (g)	2672 (723)	3109 (493)	< 0.001*
Male	15 (51.7%)	72 (48.3%)	0.737

Notes: Continuous variables are presented as median (interquartile range), and categorical variables are expressed as n (%).*P < 0.05 was considered statistically significant.
Abbreviations: PAPP-A, pregnancy-associated plasma protein A; PAPP-A2, pregnancy-associated plasma protein A2.

angle shift in the early-onset preeclampsia group (9.53 ± 4.02 mDeg) was significantly larger than that in the late-onset preeclampsia group (5.61 ± 2.50 mDeg) (P = 0.007) (Figure 3D).

Analyses of SPR Angle Shifts of Biomarkers to Predict Preeclampsia

The ROC curve analysis demonstrated optimal cut-off values of PAPP-A, PAPP-A2, and PAPP-A/PAPP-A2 ratio to predict all preeclampsia of ≤ 4.81 mDeg, > 4.59 mDeg, and ≤ 0.76, respectively (Table 2 and Figure 4A). The areas under the curves (AUCs) for PAPP-A, PAPP-A2, and PAPP-A/PAPP-A2 ratio were 0.65 (95% confidence interval (CI) 0.58–0.72, P = 0.013), 0.76 (95% CI 0.69–0.82, P < 0.001), and 0.79 (95% CI 0.73–0.85, P < 0.001), respectively. Sub-group analysis revealed optimal cut-off values of PAPP-A, PAPP-A2, and PAPP-A/PAPP-A2 ratio to predict early-onset preeclampsia of ≤ 4.81 mDeg, > 5.12 mDeg, and ≤ 0.53, respectively (Table 2 and Figure 4B). The AUCs for PAPP-A, PAPP-A2, and PAPP-A/PAPP-A2 ratio were 0.83 (95% CI 0.76–0.88, P < 0.001), 0.92 (95% CI 0.86–0.96, P < 0.001), and 0.99 (95% CI 0.96–1.00, P < 0.001), respectively. In addition, the optimal cut-off values of PAPP-A, PAPP-A2, and PAPP-A/PAPP-A2 ratio to predict late-onset preeclampsia were ≤ 4.55 mDeg, > 4.59 mDeg, and ≤ 0.73, respectively (Table 2 and Figure 4C). The AUCs for PAPP-A, PAPP-A2, and PAPP-A/PAPP-A2 ratio were 0.62 (95% CI 0.54–0.69, P = 0.089), 0.73 (95% CI 0.65–0.79, P < 0.001), and 0.75 (95% CI 0.68–0.81, P < 0.001), respectively. Through the confusion matrix, the accuracies for predicting all instances of preeclampsia were 0.75, 0.73, and 0.87 for PAPP-A, PAPP-A2, and PAPP-A/PAPP-A2 ratio, respectively. Regarding the prediction of early-onset preeclampsia, the accuracies were 0.76, 0.75, and 0.96 for PAPP-A, PAPP-A2, and PAPP-A/PAPP-A2 ratio, respectively. For late-onset preeclampsia, the accuracies were 0.76, 0.70, and 0.85 for PAPP-A, PAPP-A2, and the PAPP-A/PAPP-A2 ratio, respectively. There were statistically significant differences between PAPP-A, PAPP-A2, and PAPP-A/PAPP-A2 ratio to predict all and early-onset preeclampsia, however PAPP-A2 and PAPP-A/PAPP-A2 ratio rather than PAPP-A could predict late-onset preeclampsia (Table 2).
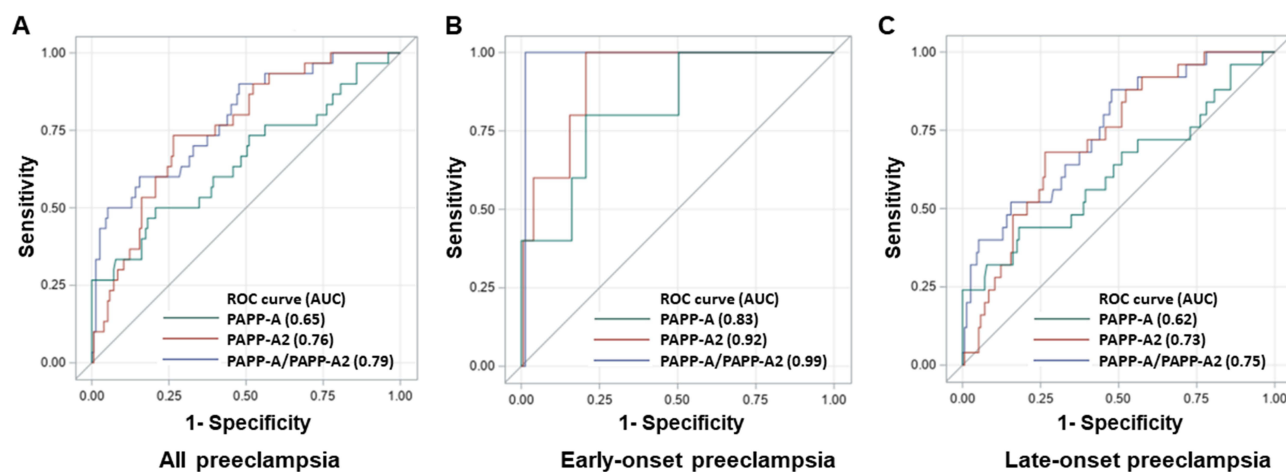
Table 2 ROC Curve Analyses of PAPP-A, PAPP-A2, and PAPP-A/PAPP-A2 Ratio for Predicting Preeclampsia

	AUC (95% CI)	Cut-off Value	Accuracy	Sensitivity	Specificity	PPV	NPV	*P* value	Detection Rate (%) For Fixed False-Positive Rate	
									5% (95% CI)	10% (95% CI)
All preeclampsia										
PAPP-A	0.65 (0.58–0.72)	≤ 4.81	0.75	0.50	0.79	0.31	0.89	0.013*	26.67 (10.00–43.33)	33.33 (18.87–53.33)
PAPP-A2	0.76 (0.69–0.82)	> 4.59	0.73	0.73	0.74	0.35	0.94	< 0.001*	13.33 (0.00–30.00)	30.00 (13.33–49.58)
PAPP-A/PAPP-A2	0.79 (0.73–0.85)	≤ 0.76	0.87	0.50	0.95	0.66	0.91	< 0.001*	46.67 (26.67–66.67)	50.00 (33.33–70.00)
Early-onset preeclampsia										
PAPP-A	0.83 (0.76–0.88)	≤ 4.81	0.76	0.80	0.79	0.11	0.99	< 0.001*	40.00 (0.00–80.00)	40.00 (0.00–80.00)
PAPP-A2	0.92 (0.86–0.96)	> 5.12	0.75	1.00	0.79	0.13	1.00	< 0.001*	60.00 (20.00–100.00)	60.00 (20.00–100.00)
PAPP-A/PAPP-A2	0.99 (0.96–1.00)	≤ 0.53	0.96	0.80	0.99	0.36	1.00	< 0.001*	100.00 (100.00–100.00)	100.00 (100.00–100.00)
Late-onset preeclampsia										
PAPP-A	0.62 (0.54–0.69)	≤ 4.55	0.76	0.44	0.82	0.28	0.90	0.089	24.00 (8.00–44.00)	32.00 (16.00–52.00)
PAPP-A2	0.73 (0.65–0.79)	> 4.59	0.70	0.68	0.74	0.30	0.93	< 0.001*	4.00 (0.00–20.00)	24.00 (4.00–44.00)
PAPP-A/PAPP-A2	0.75 (0.68–0.81)	≤ 0.73	0.85	0.36	0.95	0.43	0.89	< 0.001*	36.00 (12.00–56.00)	40.00 (20.00–56.00)

Note: *P < 0.05 was considered statistically significant.
Abbreviations: ROC, receiver operating characteristic; PAPP-A, pregnancy-associated plasma protein A; PAPP-A2, pregnancy-associated plasma protein A2; AUC, area under the curve; CI, confidence interval; PPV, positive predictive value; NPV, negative predictive value.

Figure 4 ROC curve analyses of PAPP-A, PAPP-A2, and PAPP-A/PAPP-A2 ratio for predicting preeclampsia: (**A**) All preeclampsia. The AUCs for PAPP-A, PAPP-A2, and PAPP-A/PAPP-A2 ratio are 0.65, 0.76, and 0.79. (**B**) Early-onset preeclampsia. The AUCs for PAPP-A, PAPP-A2, and PAPP-A/PAPP-A2 ratio are 0.83, 0.92, and 0.99. (**C**) Late-onset preeclampsia. The AUCs for PAPP-A, PAPP-A2, and PAPP-A/PAPP-A2 ratio are 0.62, 0.73, and 0.75.

We further compared the predictive ability of PAPP-A and PAPP-A2 for preeclampsia. Table 3 shows the ROC contrast estimation of PAPP-A and PAPP-A2 to PAPP-A/PAPP-A2 ratio for predicting preeclampsia. No significant difference was noted between PAPP-A and PAPP-A/PAPP-A-2 ratio for predicting early-onset preeclampsia, and no significant differences were noted between PAPP-A2 and PAPP-A/PAPP-A2 ratio for predicting all, early-, and late-onset preeclampsia.

Discussion

Several first-trimester screening models have been developed to predict the risk of preeclampsia. These models mainly combine maternal characteristics, biophysical and biochemical markers,[30,31] however there is currently insufficient evidence to reach a consensus on the performance and usefulness of these screening models in clinical practice.[36] Recently, several biomarkers have also been investigated with regards to their predictive ability for preeclampsia.[37] Of these biomarkers, PAPP-A has been widely used in first-trimester preeclampsia screening;[30,31] however, PAPP-A2, another potential biomarker for predicting preeclampsia, was discovered after PAPP-A, and it has not been used in clinical practice. In this study, we examined the SPR angle shifts of serum PAPP-A and PAPP-A2 in clinical samples to predict preeclampsia using a GO-SPR biosensor. We found a significantly smaller SPR angle shift for PAPP-A and a larger SPR angle shift for PAPP-A2 in the women with preeclampsia. Another significant finding of our study is that the SPR angle shift of PAPP-A2 was also substantially larger in the women who developed early-onset rather than late-onset preeclampsia.

Table 3 ROC Contrast Estimation and Testing Results of PAPP-A, PAPP-A2, and PAPP-A/PAPP-A2 Ratio

Contrast	Estimate	Standard Error	95% CI	Chi-Square	P value
All preeclampsia					
PAPP-A − (PAPP-A/PAPP-A2)	−0.14	0.04	−0.22 – (−0.06)	11.53	< 0.001*
PAPP-A2 − (PAPP-A/PAPP-A2)	−0.03	0.04	−0.12–0.05	0.56	0.456
Early-onset preeclampsia					
PAPP-A − (PAPP-A/PAPP-A2)	−0.16	0.09	−0.35–0.02	2.95	0.086
PAPP-A2 − (PAPP-A/PAPP-A2)	−0.07	0.04	−0.16–0.02	2.52	0.112
Late-onset preeclampsia					
PAPP-A − (PAPP-A/PAPP-A2)	−0.13	0.04	−0.22 – (−0.04)	8.72	0.003*
PAPP-A2 − (PAPP-A/PAPP-A2)	−0.02	0.05	−0.12–0.07	0.24	0.627

Note: *$P < 0.05$ was considered statistically significant.
Abbreviations: ROC, receiver operating characteristic; PAPP-A, pregnancy-associated plasma protein A; PAPP-A2, pregnancy-associated plasma protein A2; CI, confidence interval.

Combining biomarkers into a predictive model can enhance risk assessment compared to relying on a single biomarker. Therefore, we suggested that the PAPP-A/PAPP-A2 ratio could function as a predictive model, providing improved risk assessment compared to the use of individual PAPP-A or PAPP-A2. In addition, the cost-effectiveness of screening is another concern, and biomarker-based screening is only feasible when the accuracy is sufficiently high.[38] Under the hypothesis that it would be difficult to accurately diagnose a complex disorder such as preeclampsia using a single biomarker, we further compared the SPR angle shifts of serum PAPP-A, PAPP-A2, and PAPP-A/PAPP-A2 ratio to predict preeclampsia using the GO-SPR biosensor. The AUCs of PAPP-A measured using the GO-SPR biosensor for predicting all, early- and late-onset preeclampsia were 0.65, 0.83, and 0.62, respectively, which are better than the results of previous clinical studies using commercial biochemical assays.[39,40] We also found that the novel biomarker PAPP-A2 had higher AUCs for preeclampsia than PAPP-A, with AUCs of 0.76, 0.92, and 0.73 for predicting all, early- and late-onset preeclampsia, respectively. Furthermore, the AUCs of PAPP-A/PAPP-A2 ratio for all, early- and late-onset preeclampsia noticeably increased to 0.79, 0.99, and 0.75, respectively. Despite the limited number of cases of early-onset preeclampsia in this study, screening using the PAPP-A/PAPP-A2 ratio was particularly effective for predicting early-onset preeclampsia, which is of paramount importance because early-onset preeclampsia is associated with more adverse maternal and perinatal outcomes than late-onset preeclampsia.[2,41]

Despite having higher AUCs than PAPP-A, PAPP-A2 exhibited lower detection rates in predicting all and late-onset preeclampsia in this study. This divergence suggests that while PAPP-A2 excels in distinguishing between outcomes, it may be less effective in identifying positive cases within these specific categories. Potential influencing factors include intrinsic characteristics of the biomarkers and their nuanced performance in differentiating between diverse subtypes of preeclampsia. Further exploration and potential adjustments are necessary to optimize the predictive accuracy of PAPP-A2 for all and late-onset preeclampsia.

The ROC contrast estimation showed no significant differences between PAPP-A and the PAPP-A/PAPP-A2 ratio in predicting early-onset preeclampsia. Additionally, no distinctions were observed between PAPP-A2 and the PAPP-A/PAPP-A2 ratio for predicting all, early-, and late-onset preeclampsia. This suggests comparable performance between PAPP-A and the PAPP-A/PAPP-A2 ratio in predicting early-onset preeclampsia, with neither showing superiority. Likewise, PAPP-A2 and the PAPP-A/PAPP-A2 ratio demonstrated similar performance in predicting all, early-, and late-onset preeclampsia, with no clear superiority of one over the other. Consequently, based on the results, the PAPP-A/PAPP-A2 ratio emerged as the best predictor among the three biomarkers, as it exhibited the highest AUCs for all three preeclampsia subtypes and was not significantly worse than PAPP-A or PAPP-A2 for any specific outcome. While the sensitivity of the PAPP-A/PAPP-A2 ratio has not been sufficiently high, the specificity and accuracy of this ratio were markedly superior to those of PAPP-A and PAPP-A2. High specificity reduces the number of false positives, which can result in unnecessary medical interventions, additional testing, and undue stress for pregnant individuals.

In this study, we utilized the PAPP-A/PAPP-A2 ratio to predict preeclampsia. The inherent characteristic of employing ratios underscores proportional changes over absolute changes. A limitation arises from the fact that alterations in the numerator or denominator can yield the same ratio. Consequently, we conducted distinct analyses to scrutinize the individual contributions of PAPP-A and PAPP-A2, offering a more comprehensive perspective on the data. These supplementary analyses complement our primary approach and contribute to a broader understanding of the dataset.

Various biosensors for early detection of preeclamptic biomarkers have become available in recent years, such as DNA aptamer, Au nanoparticle, dendrimers, and graphene based immunosensors, carboxylated polypyrrole nanotube, glassy carbon electrode, piezoelectric quartz, carbon nanotube, SPR, nanoporous microneedle array, and nanoscale field effect transistor.[11–17] Li et al used a functional single walled carbon nanotubes/chitosan-based electrochemical immunosensor to detect PAPP-A with a limit of detection (LOD) of 39 ng/mL.[12] Bocková et al used a SPR-based sandwich assay with functionalized Au nanoparticles to detect PAPP-A2 in 30% blood plasma with a LOD of 3.6 ng/mL.[13] Kang et al demonstrated an immuno-functionalized nanoporous microneedle array to detect estrogen for diagnosis of preeclampsia with a LOD of 0.5 ng/mL.[14] Pham et al used a point-of-care platform based on nanoscale indium oxide field effect transistor to measure placental growth factor for diagnosis of preeclampsia with a LOD of 0.06 pg/mL.[15] Our previous studies also demonstrated the GO-based SPR biosensor to measure both PAPP-A and PAPP-A2 with LODs of 0.5 ng/mL, and the carboxyl-GO-based SPR biosensor to detect PAPP-A2 with a LOD as low as 0.01 pg/mL.[16,17] Moreover, our

previous experiment demonstrated a low level of cross-reactivity between PAPP-A and PAPP-A2 when employing the GO-based SPR.[17]

In clinical practice, the most common method to detect biomarkers is ELISA. However, the disadvantages of ELISA include that it is a time-consuming procedure (due to the labeling and detection steps), high purchase cost, cross-reactivity with secondary antibodies, and decay of color signal intensity. The TRACE method is an improvement on ELISA to obtain more precise results, however it also requires multiple intermediate steps (such as washing or the addition of solutions) and the cost of reagents and instrumentation is high. In contrast to these commercial assays, the GO-based SPR biosensor has the benefits of being label-free, rapid, and low-cost, and also that it can provide real-time results. The GO films are functionalized SAMs on amino-modified Au surfaces by the linker of cystamine, and the physical displacements are established between protein-protein interactions, protein affinity adsorption forces, and protein binding forces. Our previous studies have demonstrated that GO provides ideal bio-affinity, stable carbon molecular structures, and enhanced plasmon resonance energy at the sensor-protein interface.[25,28,34] We also demonstrated the thin-film design and analysis of plasmonic modes using the Essential Macleod software package and confirmed the GO-based SPR biosensor structure can increase the electric field propagation distance and penetration depth of the interface.[35] We have obtained a US patent (US20190212263A1) for the GO-based SPR chip, and the commercialization process is currently underway. The SPR chip is priced in the range of $50 to $100, and its value is augmented by its reusability and suitability for multichannel detection. These chips can be efficiently mass-produced at a lower cost in a dedicated optical fabrication facility.

In this pilot study, we successfully demonstrated that measuring the first-trimester serum PAPPA/PAPPA2 ratio by the GO-based SPR biosensor could predict preeclampsia in pregnant women in a clinical setting. However, owing to the prospective nature of the study, the incidence of early-onset preeclampsia was relatively low, constituting a limitation in the study. Additional larger prospective cohort studies are essential to validate our preliminary results.

Conclusion

Our study revealed that there is an association between the first-trimester serum PAPP-A/PAPP-A2 ratio and the prediction of preeclampsia using the GO-based SPR biosensor. The GO-SPR biosensor might be a potential alternative to conventional methods such as ELISA. Furthermore, adding PAPP-A/PAPP-A2 ratio screening to current screening models could more accurately predict pregnant women at risk of developing preeclampsia. This would allow health care providers to perform prophylactic procedures, monitor the progression of disease at an early stage, and thereby optimize the time of delivery to ameliorate maternal and perinatal outcomes. Moreover, the early identification of women at low risk of preeclampsia women can reduce their anxiety, avoid unnecessary hospitalization and reduce unnecessary medical care costs.

Funding

Disclosure

The authors report no conflicts of interest in this work.

References

1. Steegers EA, von Dadelszen P, Duvekot JJ, et al. Pre-eclampsia. *Lancet*. 2010;376:631–644. doi:10.1016/S0140-6736(10)60279-6
2. Burton GJ, Redman CW, Roberts JM, et al. Pre-eclampsia: pathophysiology and clinical implications. *BMJ*. 2019;366:I2381. doi:10.1136/bmj.l2381.
3. Rana S, Lemoine E, Granger JP, et al. Preeclampsia: pathophysiology, challenges, and perspectives. *Circ Res*. 2019;124:1094–1112. doi:10.1161/CIRCRESAHA.118.313276
4. Giudice LC, Martina NA, Crystal RA, et al. Insulin-like growth factor binding protein-1 at the maternal-fetal interface and insulin-like growth factor-I, insulin-like growth factor-II, and insulin-like growth factor binding protein-1 in the circulation of women with severe preeclampsia. *Am J Obstet Gynecol*. 1997;176:751–757. doi:10.1016/S0002-9378(97)70598-2
5. Boldt HB, Overgaard MT, Laursen LS, et al. Mutational analysis of the proteolytic domain of pregnancy-associated plasma protein-A (PAPP-A): classification as a metzincin. *Biochem J*. 2001;358:359–367. doi:10.1042/bj3580359

6. Overgaard MT, Boldt HB, Laursen LS, et al. Pregnancy-associated plasma protein-A2 (PAPP-A2), a novel insulin-like growth factor-binding protein-5 proteinase. *J Biol Chem*. 2001;276:21849–21853. doi:10.1074/jbc.M102191200

7. Poon LC, Maiz N, Valencia C, et al. First-trimester maternal serum pregnancy-associated plasma protein-A and pre-eclampsia. *Ultrasound Obstet Gynecol*. 2009;33:23–33. doi:10.1002/uog.6280

8. Hourrier S, Salomon LJ, Dreux S, et al. Screening for adverse pregnancy outcome at early gestational age. *Clin Chim Acta*. 2010;411:1547–1552. doi:10.1016/j.cca.2010.06.024

9. Crosley EJ, Durland U, Seethram K, et al. First-trimester levels of pregnancy-associated plasma protein A2 (PAPP-A2) in the maternal circulation are elevated in pregnancies that subsequently develop preeclampsia. *Reprod Sci*. 2014;21:754–760. doi:10.1177/1933719113512532

10. Neuman RI, Alblas van der Meer MM, Nieboer D, et al. PAPP-A2 and inhibin A as novel predictors for pregnancy complications in women with suspected or confirmed preeclampsia. *J Am Heart Assoc*. 2020;9:e018219.

11. Suman P, Gandhi S, Kumar P, et al. Prospects of electrochemical immunosensors for early diagnosis of preeclampsia. *Am J Reprod Immunol*. 2017;77. doi:10.1111/aji.12584

12. Li J, Liu G, Zhang W, et al. Competitive detection of pregnancy-associated plasma protein-A in serum using functional single walled carbon nanotubes/chitosan-based electrochemical immunosensor. *J Electroanal Chem*. 2013;708:95–100. doi:10.1016/j.jelechem.2013.09.026

13. Bocková M, Chadtová Song X, Gedeonová E, et al. Surface plasmon resonance biosensor for detection of pregnancy associated plasma protein A2 in clinical samples. *Anal Bioanal Chem*. 2016;408:7265–7269. doi:10.1007/s00216-016-9664-z

14. Kang YE, Seong KY, Yim SG, et al. Nanochannel-driven rapid capture of sub-nanogram level biomarkers for painless preeclampsia diagnosis. *Biosens Bioelectron*. 2020;163:112281. doi:10.1016/j.bios.2020.112281

15. Pham TTT, Tran DP, Nguyen MC, et al. A simplified point-of-care testing approach for preeclampsia blood biomarkers based on nanoscale field effect transistors. *Nanoscale*. 2021;13:12279–12287. doi:10.1039/D1NR02461B

16. Chiu NF, Tai MJ, Wu HP, et al. Development of a bioaffinity SPR immunosensor based on functionalized graphene oxide for the detection of pregnancy-associated plasma protein A2 in human plasma. *Int J Nanomedicine*. 2019;14:6735–6748. doi:10.2147/IJN.S213653

17. Fan SY, Chiu NF, Chen CP, et al. Simultaneous real-time detection of pregnancy-associated plasma protein-A and -A2 using a graphene oxide-based surface plasmon resonance biosensor. *Int J Nanomedicine*. 2020;15:2085–2094. doi:10.2147/IJN.S237938

18. Reina G, González-Domínguez JM, Criado A, et al. Promises, facts and challenges for graphene in biomedical applications. *Chem Soc Rev*. 2017;46:4400–4416. doi:10.1039/C7CS00363C

19. Hegab HM, ElMekawy A, Zou L, et al. The controversial antibacterial activity of graphene-based materials. *Carbon*. 2016;105:362–376. doi:10.1016/j.carbon.2016.04.046

20. Liu J, Cui L, Losic D. Graphene and graphene oxide as new nanocarriers for drug delivery applications. *Acta Biomater*. 2013;9:9243–9257.

21. Chung C, Kim YK, Shin D, et al. Biomedical applications of graphene and graphene oxide. *Acc Chem Res*. 2013;46:2211–2224. doi:10.1021/ar300159f

22. Velasco-Soto MA, Pérez-García SA, Alvarez-Quintana J, et al. Selective band gap manipulation of graphene oxide by its reduction with mild reagents. *Carbon*. 2015;93:967–973. doi:10.1016/j.carbon.2015.06.013

23. Chiu NF, Yang CD. Real-time and stepwise deoxidization processes to tune the photoluminescence properties of graphene oxide using EC-SPR spectroscopy. *RSC Adv*. 2018;8:11557–11565. doi:10.1039/C7RA13594G

24. Chiu NF, Fan SY, Yang CD, et al. Carboxyl-functionalized graphene oxide composites as SPR biosensors with enhanced sensitivity for immunoaffinity detection. *Biosens Bioelectron*. 2017;89:370–376. doi:10.1016/j.bios.2016.06.073

25. Chiu NF, Wang YH, Chen CY. Clinical application for screening down's syndrome by using carboxylated graphene oxide-based surface plasmon resonance aptasensors. *Int J Nanomedicine*. 2020;15:8131–8149. doi:10.2147/IJN.S270938

26. Shang J, Ma L, Li J, et al. The origin of fluorescence from graphene oxide. *Sci Rep*. 2012;2:792. doi:10.1038/srep00792

27. Zheng P, Wu N. Fluorescence and sensing applications of graphene oxide and graphene quantum dots: a review. *Chem Asian J*. 2017;12:2343–2353. doi:10.1002/asia.201700814

28. Chiu NF, Huang TY, Lai HC, et al. Graphene oxide-based SPR biosensor chip for immunoassay applications. *Nanoscale Res Lett*. 2014;9:445. doi:10.1186/1556-276X-9-445

29. Rolnik DL, Wright D, Poon LC, et al. Aspirin versus placebo in pregnancies at high risk for preterm preeclampsia. *N Engl J Med*. 2017;377:613–622. doi:10.1056/NEJMoa1704559

30. Poon LC, Shennan A, Hyett JA, et al. The International Federation of Gynecology and Obstetrics (FIGO) initiative on pre-eclampsia: a pragmatic guide for first-trimester screening and prevention. *Int J Gynaecol Obstet*. 2019;145(Suppl 1):1–33. doi:10.1002/ijgo.12802

31. Chaemsaithong P, Sahota DS, Poon LC. First trimester preeclampsia screening and prediction. *Am J Obstet Gynecol*. 2022;226:S1071–97.e2.

32. American College of Obstetricians and Gynecologists. Gestational hypertension and preeclampsia: ACOG practice bulletin, number 222. *Obstet Gynecol*. 2020;135:e237–e260. doi:10.1097/AOG.0000000000003891

33. Chiu NF, Kuo CT, Lin TL, et al. Ultra-high sensitivity of the non-immunological affinity of graphene oxide-peptide-based surface plasmon resonance biosensors to detect human chorionic gonadotropin. *Biosens Bioelectron*. 2017;94:351–357. doi:10.1016/j.bios.2017.03.008

34. Chiu NF, Huang TY. Sensitivity and kinetic analysis of graphene oxide-based surface plasmon resonance biosensors. *Sens Actuators B Chem*. 2014;197:35–42. doi:10.1016/j.snb.2014.02.033

35. Chiu NF, Lin TL, Kuo CT. Highly sensitive carboxyl-graphene oxide-based surface plasmon resonance immunosensor for the detection of lung cancer for cytokeratin 19 biomarker in human plasma. *Sens Actuators B Chem*. 2018;265:264–272. doi:10.1016/j.snb.2018.03.070

36. Kleinrouweler CE, Cheong-See FM, Collins GS, et al. Prognostic models in obstetrics: available, but far from applicable. *Am J Obstet Gynecol*. 2016;214:79–90.e36. doi:10.1016/j.ajog.2015.06.013

37. Wu P, van den Berg C, Alfirevic Z, et al. Early pregnancy biomarkers in pre-eclampsia: a systematic review and meta-analysis. *Int J Mol Sci*. 2015;16:23035–23056. doi:10.3390/ijms160923035

38. Zakiyah N, Postma MJ, Baker PN, et al. Pre-eclampsia diagnosis and treatment options: a review of published economic assessments. *Pharmacoeconomics*. 2015;33:1069–1082. doi:10.1007/s40273-015-0291-x

39. Audibert F, Boucoiran I, An N, et al. Screening for preeclampsia using first-trimester serum markers and uterine artery Doppler in nulliparous women. *Am J Obstet Gynecol*. 2010;203:383.e1–8. doi:10.1016/j.ajog.2010.06.014

40. Pihl K, Sørensen S, Stener Jørgensen F. Prediction of preeclampsia in nulliparous women according to first trimester maternal factors and serum markers. *Fetal Diagn Ther.* 2020;47:277–283. doi:10.1159/000503229
41. van Esch JJA, van Heijst AF, de Haan AFJ, et al. Early-onset preeclampsia is associated with perinatal mortality and severe neonatal morbidity. *J Matern Fetal Neonatal Med.* 2017;30:2789–2794. doi:10.1080/14767058.2016.1263295